Building change detection using multi-sensor and multi-view-angle imagery

S Jabari and Y Zhang

[1] CRC-AGIP Lab, Department of Geodesy and Geomatics Engineering, University of New Brunswick, Fredericton, NB, Canada

E-mail: sh.jabari@unb.ca

Abstract. Change detection of buildings in urban areas is very challenging due to geometric distortions in very high resolution (VHR). These distortions create problems in the co-registration of different images. Thus, it is very problematic to exploit images acquired by different sensors and different view angles using conventional change detection methods. Therefore, the majority of studies in this field avoid using multi-sensor and multi-view angle images. In this study, a novel co-registration method, called Patch-Wise Co-Registration (PWCR), is used to contribute to a solution of the problem. This method integrates the sensor model parameters into the co-registration process to relate corresponding pixels. From the corresponding pixels, corresponding segments (patches) are generated. Later on, the brightness values of the matching pixels/segments are compared in order to detect changes. Here, a Multivariate Alteration Detection (MAD) transform is used for identifying the changed segments. The proposed method provides the opportunity to utilize various images as bi-temporal sets for change detection.

1. Introduction

Building change detection matters to a large number of organizations, such as municipalities and local governments, for a wide range of applications including map updating and hazard assessment. Very high resolution (VHR) satellite images have been increasingly used for building change detection since they provide adequate details for this purpose.

The majority of change detection studies reported in the literature take a 2D approach for this purpose (Al-Khudhairy et al., 2005; Bouziani et al., 2010; Im et al., 2008; Im & Jensen, 2005; Zhou et al., 2008). The studies in this category either ignore the effect of relief distortion by selecting a flat area (Im & Jensen, 2005) for the study or use ortho-rectified images (Bouziani et al., 2007).

There is a second group of studies that deal with urban change detection using a 3D approach, in which bi-temporal Digital Surface Models (DSMs) associated with the bi-temporal images of the study area are compared to detect changes (Jung, 2004; Martha et al., 2010; Murakami et al., 1999; Tian et al., 2014).

The work of Pollard et al. (2010) is representative of the third group of studies. They use a voxel-based approach for change detection that considers each image as an instance of a volumetric space with intensities following a Bayesian probability theory. The intensities are updated every time a new image is introduced to the system (Crispell et al., 2012; Kang et al., 2013). This method requires

Content from this work may be used under the terms of the Creative Commons Attribution 3.0 licence. Any further distribution of this work must maintain attribution to the author(s) and the title of the work, journal citation and DOI.
Published under licence by IOP Publishing Ltd

several images to get the system trained; it is not possible to apply it to the bi-temporal images. According to the literature, no solution has been found that can effectively co-register bi-temporal VHR images acquired from different viewing angles and different sensors and detect urban changes at object level.

Nowadays, most satellite images produced by VHR sensors are acquired under off-nadir angle viewing conditions. On the other hand, many developed cities also acquire airborne images for city monitoring purposes on a regular basis. Being able to combine these images for building change detection is of great benefit and can help to reduce cost.

Considering that almost all of the VHR images acquired from the same area are taken from varying view-angles, the layout of the elevated objects in bi- or multi-temporal imagery is different. Moreover, although satellite images and airborne images visually appear similar, they have distinctly different imaging geometries. Normally, VHR satellite images are acquired using push broom sensors. They have a line-perspective geometry, whereas most airborne images have a center perspective geometry. This geometric difference causes a significant problem in co-registration of satellite and airborne images and presents challenges for change detection.

In order to utilize the combination of off-nadir VHR satellite and airborne images for urban change detection and to overcome the problem of global co-registration, we developed in our previous research a Patch-Wise Co-Registration (PWCR) approach to co-register corresponding patches in bi-temporal satellite images. This approach uses Rational Polynomial Coefficients (RPCs) of satellite images and the DSM of the area to guide the patch registration. Then, changes in bi-temporal VHR satellite images are identified by comparing the co-registered patches (Jabari & Zhang, 2015).

In this study, we use a PWCR-MAD approach to detect building changes using bi-temporal images selected from large off-nadir angle satellite images and aerial photos at different spatial resolutions. Beside the RPC parameters of satellite images and a DSM of the area, we also include the exterior orientation parameters of airborne images in the sensor modeling to regenerate the imaging conditions for both satellite and airborne images at different scales so that the images can be co-registered in a patch-wise manner. Then, the Multivariate Alteration Detection (MAD) transform (Nielsen et al., 1998) is utilized to detect changed patches (segments).

With the method presented in this paper, images with similar spectral sensor properties can be used in building change detection and the difference in the geometry does not cause problems.
Since buildings in satellite and airborne sensor images are tilted in different directions because of the varying off-nadir angles and the projection differences change detection in this study is limited to detect building roof changes, as the different images may display different facades of a particular building.

2. Methodology

The methodology in the paper is divided into two major steps, which are explained in detail in the following subsections: Patch-Wise Co-Registration (PWCR), with the purpose to find corresponding segments (patches) in the bi-temporal images; and Spectral Properties Comparison, which compares the spectral properties of the corresponding patches (segments) using a Multivariate Alteration Detection (MAD) transform to detect changes.

1.1 Patch-Wise Co-Registration

The goal of the PWCR is to take a segment (patch) from the base image and transfer it to its corresponding place in the target image in such a way that the both segments represent the exact same object or part of the object (Jabari & Zhang, 2015).

1.1.1 Segmentation

In this stage, one of the bi-temporal images is considered to be the base image and is segmented so that each segment has a unique ID. In this study, we used the previously available building borders as a thematic layer. The rest of the image is segmented using the multi-resolution segmentation method.

1.1.2 Co-Registered Segment Generation

The corresponding points, and accordingly segments, are detected by using the DSM points. In satellite images the DSM projection is done using RFM equations (1):

$$\tilde{x} = \frac{P_1(X,Y,Z)}{P_2(X,Y,Z)}$$

$$\tilde{y} = \frac{P_3(X,Y,Z)}{P_4(X,Y,Z)}$$

$$P(X,Y,Z) = \sum_{c=0}^{m}\sum_{b=0}^{m}\sum_{a=0}^{m} A_{a,b,c} X^a Y^b Z^c \quad (1)$$

where $\tilde{x}$ and $\tilde{y}$ are normalized image coordinates, and X, Y, and Z are normalized ground coordinates. m is generally set to 3 (Grodecki, 2001). Here, we need to use bias compensated RPCs as presented by (Fraser & Hanley, 2003). This is to prevent ephemeris errors to affect the accuracy of image coordinates.

In airborne images, the collinearity equations (2) are used:

$$\begin{aligned} x &= x_0 - f\frac{(X-X_o)m_{11} + (Y-Y_o)m_{12} + (Z-Z_o)m_{13}}{(X-X_o)m_{31} + (Y-Y_o)m_{32} + (Z-Z_o)m_{33}} \\ y &= y_0 - f\frac{(X-X_o)m_{21} + (Y-Y_o)m_{22} + (Z-Z_o)m_{23}}{(X-X_o)m_{31} + (Y-Y_o)m_{32} + (Z-Z_o)m_{33}} \end{aligned} \quad (2)$$

where, x_0 and y_0 are principal point image coordinates; X_o, Y_o, and Z_o are principal point object coordinates, generally measured by onboard mounted GPS; m_{ij} are the entries of the rotation matrix, that are given in Equation 3.

$$M = \begin{bmatrix} \cos(\varphi)\cos(\kappa) & -\cos(\varphi)\sin(\kappa) & \sin(\varphi) \\ \cos(\omega)\sin(\kappa) + \sin(\omega)\sin(\varphi)\cos(\kappa) & \cos(\omega)\cos(\kappa) - \sin(\omega)\sin(\varphi)\sin(\kappa) & -\sin(\omega)\cos(\varphi) \\ \sin(\omega)\sin(\kappa) - \cos(\omega)\sin(\varphi)\cos(\kappa) & \sin(\omega)\cos(\kappa) + \cos(\omega)\sin(\varphi)\sin(\kappa) & \cos(\omega)\cos(\varphi) \end{bmatrix} \quad (3)$$

where, M is the rotation matrix; $\omega, \varphi,$ and κ are sensor rotation angles around X, Y, and Z axis, respectively, which are generally measured by onboard mounted Inertial Measurement Unit (IMU). The projected points and the original points are expected to be the same, provided that the errors of DSM and exterior orientation parameters are negligible.

Having used DSM pixels, the corresponding points in images are detected. So, the corresponding segments in the target image are generated.

1.2 Spectral Comparison

In this study, a MAD transform is used for spectral comparison of the co-registered segments in order to detect changes. The better performance of MAD compared to principal component analysis has previously been proved by (Nielsen et al.,1998). This method generates a linear transformation of the radiometric content of the pixels/segments and benefits from canonical coefficients to maximize the disparity between the brightness values in bi-temporal images. It transfers the bi-temporal spectral

vectors $X = [X_1, \dots, X_k]^T$ and $Y = [Y_1, \dots, Y_k]^T$, k being the number of the spectral bands, into the space D (Nielsen, 2011),

$$D = a^T X - b^T Y \quad (4)$$

in which a and b are the coefficients of a linear combination of the spectral bands so that $Var\{a^T X - b^T Y\}$ is maximized with constraints $Var\{a^T X\} = Var\{b^T Y\} = 1$. This formulation is solved using the Canonical Correlation Analysis. The Canonical Correlation Analysis transfers two vectors into a new space which is a linear combination of the original space. The first set of coefficients provides the highest correlation which is equal to the lowest variation (${a^T}_1 X - {b^T}_1 Y$). The second set provides the second highest correlation. And the k^{th} set generates the highest variance (${a^T}_k X - {b^T}_k Y$) (Nielsen, 2011),

$$\begin{bmatrix} X \\ Y \end{bmatrix} \rightarrow \begin{bmatrix} {a^T}_k X - {b^T}_k Y \\ \vdots \\ . \\ {a^T}_1 X - {b^T}_1 Y \end{bmatrix} \quad (5)$$

$$D\{a^T X - b^T Y\} = 2(I - R)$$

where, I is the $k \times k$ unit matrix and R is a $k \times k$ diagonal matrix containing the sorted canonical correlations on the diagonal.

2. Study Area

In this study, the presented PWCR-MAD change detection method is tested on a combination of airborne and satellite images collected over the city of Fredericton, NB, Canada. Table 1 shows the main specifications of the imagery. Table 2 specifies the bi-temporal combinations.

Table 1: The general specifications of the images used for change detection in this study

Dataset ID	WV2-2011	WV2-2013	AB-1	AB-2
Satellite	Wordview2	Wordview2	Airborne	Airborne
City and country	Fredericton Canada	Fredericton Canada	Fredericton Canada	Fredericton Canada
Date	7/20/2011	8/18/2013	2005	2005
Approx. GSD (m)	0.495	0.582	0.5	0.5
Mean ONA (deg)	15	27.1	-	-
Number of spectral bands	8	8	3 (RGB)	3 (RGB)

Table 2: The bi-temporal combination of the satellite images used for change detection in this study and the unique specifications of the bi-temporal combination

Dataset ID	Base image	Target image	Specification	DSM Source
DT1	WV2-2011	WV-2-2013	Combination of two off-nadir satellite images	LiDAR(0.5m accuracy)
DT2	WV2-2011	AB-1	Combination of off-nadir satellite image and airborne image	LiDAR(0.5m accuracy)
DT3	WV2-2011	AB-2	Combination of off-nadir satellite image and airborne image	LiDAR(0.5m accuracy)

3. Results

3.1 Co-registration results

Figure 1 shows two samples of building borders in the base image (a and e) and the ones transferred to the target images using the PWCR method (b to d) and (f to h). As illustrated in figure 1, the PWCR has been able to detect the proper building borders, although the buildings lean to different sides in different images. At the time of acquisition time of the images in figure 1 (g) and (h), the building had not been constructed yet; therefore, the border is transferred to the position where the building was later constructed, and where its roof outline could have been found. Note that figure 1 (a) and (e) are two buildings segments in the WV2-2011 image, constituting a base image in datasets DT1, DT2, and DT3. For illustration purpose, the building segments in (a) and € are edited manually to fit the building borders. In (b) and (f) the segments are transferred from the base image to the WV2-2013 image (target image in DT1). In (c) and (g) the segments are transferred from the base image to the AB-1 image (target image in DT2). In (d) and (h) the segments are transferred from the base image to the AB-2 image (target image in DT3). In (g) and (h), since the target images are taken six years before the base image, the building in (e) does not exist in (g) and (h); the highlighted area represents the border of the building if it existed at the time of the image acquisition.

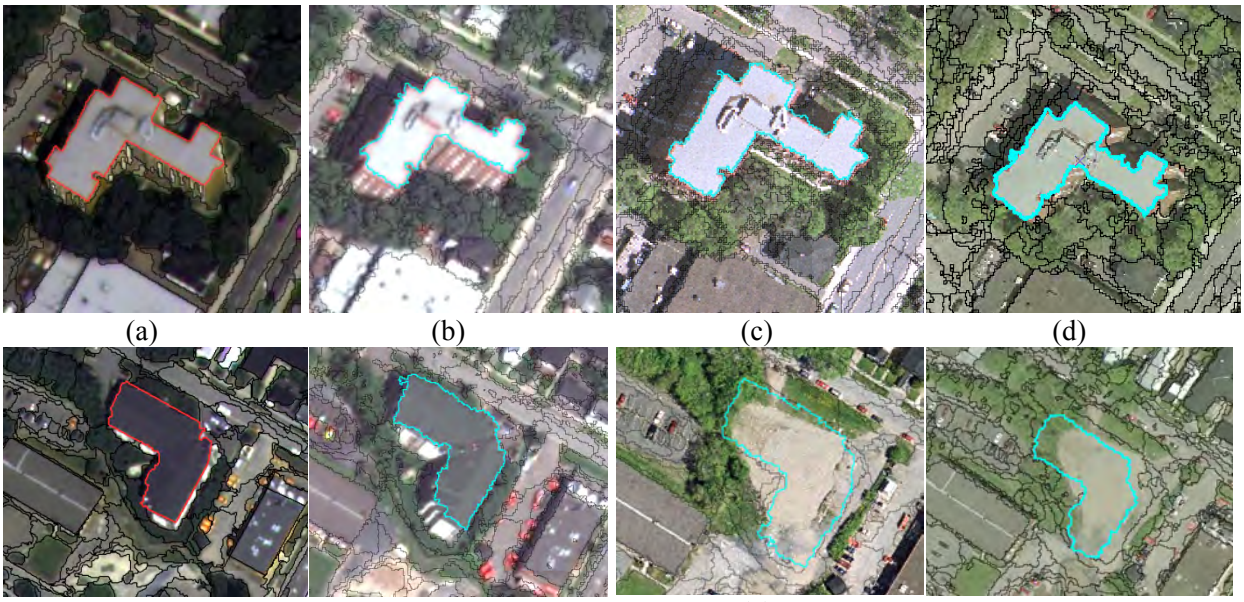


Figure 1: Samples of the borders of two elevated buildings in the Fredericton images showing the ability of the co-registration method to transfer segments from one image to their precise position in the other image. (Source of imagery: Worldview-2 and LiDAR)

3.2 Change Detection Results

As presented in Canty (2014) and Fraser & Hanley (2003), the optimum threshold for MAD results is given by$\pm 2\sigma_M$, where $\sigma_M$is the standard deviation of the MAD bands. We took this value as the change threshold and checked the produced building change labels against manually generated change labels of samples of buildings to calculate the accuracy of the produced change detection results. Table 3 shows the confusion matrix generated for each dataset.

Table 3: Confusion matrix of datasets DT1 to DT3

Dataset ID		DT3		DT2		DT1	
Confusion Matrix	Changed	10	1	10	2	11	1
	Unchanged	3	33	3	31	2	37
Overall Accuracy		0.91		0.89		0.94	

4. Discussion

As can be seen from the results, the PWCR method was able to detect building borders in bi-temporal images even where the geometric properties and view angles of the images are different. The use of a MAD transform presented high accuracies in identifying changes from non-changed buildings with an overall accuracy over 90%.

In dataset DT1 there are 8 spectral bands; therefore higher change detection accuracy is achieved, while in datasets DT2 and DT3, since only 3 bands are used for change detection, lower accuracy is generated. The more the number of independent bands, the higher is the expected change detection accuracy.

5. Conclusion

In this study, we presented a building change detection method employing images with various geometries, including close-to-nadir, off-nadir, and airborne images, which are rarely considered in conventional methods of automatic and semi-automatic change detection and bi-temporal dataset selection.

Because of geometric differences in the bi-temporal images used in this study as well as relief displacement in the buildings, direct co-registration of the VHR images is not possible. Thus, considering the 3D object information (using a DSM) and the orientation properties of the images (image-object coordinate relations), PWCR was established. The DSM was used for relating the matching points and thus generating the matching segments. Then, using a MAD transform, the spectral properties of the matching segments were compared in order to detect the changes.

From the achieved results it can be concluded that the combination of PWCR and MAD transform can perform properly in building change detection using a wide range of images from close-to-nadir to off-nadir and even airborne images, provided that the spectral bands are similar.

6. References

[1] Al-Khudhairy, D., Caravaggi, I. and Glada, S. 2005 Structural damage assessments from ikonos data using change detection, object-oriented segmentation, and classification techniques. *Photogrammetric Engineering and Remote Sensing* ***71*** (7) 825-837.

[2] Bouziani M., Goïta K. and He D.C. 2010 Automatic change detection of buildings in urban environment from very high spatial resolution images using existing geodatabase and prior knowledge. *ISPRS Journal of Photogrammetry and Remote Sensing* ***65*** 143-153.

[3] Bouziani, M., Goïta, K. and He, D. C. 2007 Change detection of buildings in urban environment from high spatial resolution satellite images using existing cartographic data and prior knowledge. *IEEE International Geoscience and Remote Sensing Symposium,* Barcelona, 2581-2584.

[4] Canty, M. J. 2014 *Image analysis, classification and change detection in remote sensing: With algorithms for ENVI/IDL and python.* CRC Press.

[5] Crispell, D., Mundy, J. and Taubin, G. 2012 A variable-resolution probabilistic three-dimensional model for change detection. *IEEE Trans. Geoscience and Remote Sensing* ***50*** (2) 489-500.

[6] Fraser, C. S. and Hanley, H. B. 2003 Bias compensation in rational functions for ikonos satellite imagery. *Photogrammetric Engineering & Remote Sensing* ***69*** (1) 53-57.
[7] Grodecki, J. 2001 Ikonos stereo feature extraction-RPC approach. *Annual Conference of the ASPRS 2001,* Missouri, 23-27.
[8] Im, J., Jensen, J. and Tullis, J. 2008 Object-based change detection using correlation image analysis and image segmentation. *International Journal of Remote Sensing* ***29*** (2) 399-423.
[9] Im, J., & Jensen, J. R. 2005 A change detection model based on neighborhood correlation image analysis and decision tree classification. *Remote Sensing of Environment* ***99*** (3) 326-340.
[10] Jabari, S. and Zhang, Y. 2015 RPC-based co-registration of VHR imagery for urban change detection. *in prep.: PE&RS,*
[11] Jung, F. 2004 Detecting building changes from multitemporal aerial stereopairs. *ISPRS Journal of Photogrammetry and Remote Sensing* ***58*** (3) 187-201.
[12] Kang, Z., Zhang, L., Yue, H. and Lindenbergh, R. 2013 Range image techniques for fast detection and quantification of changes in repeatedly scanned buildings. *Photogrammetric Engineering & Remote Sensing* ***79*** (8) 695-707.
[13] Martha, T. R., Kerle, N., Jetten, V., van Westen, C. J. and Kumar, K. V. 2010 Landslide volumetric analysis using cartosat-1-derived DEMs. *Geoscience and Remote Sensing Letters, IEEE* ***7*** (3) 582-586.
[14] Murakami, H., Nakagawa, K., Hasegawa, H., Shibata, T., & Iwanami, E. 1999 Change detection of buildings using an airborne laser scanner. *ISPRS Journal of Photogrammetry and Remote Sensing* ***54*** (2) 148-152.
[15] Nielsen, A. A., Conradsen, K. and Simpson, J. J. 1998 Multivariate alteration detection (MAD) and MAF postprocessing in multispectral, bitemporal image data: New approaches to change detection studies. *Remote Sensing of Environment* ***64*** (1), 1-19.
[16] Nielsen, A. A. 2011 Kernel maximum autocorrelation factor and minimum noise fraction transformations. *IEEE Transactions on Image Processing* ***20*** (3) 612-624.
[17] Pollard, T. B., Eden, I., Mundy, J. L. and Cooper, D. B 2010 A volumetric approach to change detection in satellite images. *Photogrammetric Engineering & Remote Sensing* ***76*** (7) 817-831.
[18] Tian, J., Cui, S. and Reinartz, P. 2014 Building change detection based on satellite stereo imagery and digital surface models. *IEEE Trans. Geoscience and Remote Sensing* ***52*** (1) 406-417.
[19] Zhou, W., Troy, A. and Grove, M. 2008 Object-based land cover classification and change analysis in the Baltimore metropolitan area using multitemporal high resolution remote sensing data. *Sensors* ***8*** (3) 1613-1636.